Available online at www.sciencedirect.com
SCIENCE DIRECT®
Chemical Physics 294 (2003) 211–220
Chemical Physics
www.elsevier.com/locate/chemphys

A computational study on $Cu_nN^{0,\pm1}$ ($n = 1$–4) clusters by density functional methods

Ju-Guang Han [a,b,c,*], Liu-Si Sheng [a], Yun-Wu Zhang [a], Jorge A. Morales [c]

[a] National Synchrotron Radiation Laboratory, University of Science and Technology of China, Hefei 230026, PR China
[b] Structural Research Laboratory and the Key Laboratory of Structural Biology, University of Science and Technology of China, Chinese Academy of Sciences, Hefei 230027, PR China
[c] Department of Chemistry and Biochemistry, Texas Tech University, P.O. Box 41061, Lubbock, TX 79409-1061, USA

Received 4 August 2002; accepted 7 August 2003

Abstract

Clusters of the type $Cu_nN^{0,\pm1}$ ($n = 1$–4) are investigated computationally using density functional theory methods. Equilibrium geometries are optimized under the constraint of well-defined point-group symmetries at the B3LYP level employing a pseudo-potential method in conjunction with double-zeta basis sets. In this article, different molecular properties such as total energies, electron affinities, ionization potentials, fragmentation energies and equilibrium geometries of the $Cu_nN^{0,\pm1}$ ($n = 1$–4) clusters are systematically calculated and discussed. In particular, the photoelectron spectra of the anionic Cu_nN^{-1} ($n = 2$–4) clusters are calculated showing a good agreement with the available experimental results. In addition, Mulliken and natural orbital population analyses, and natural orbital configurations are calculated in order to elucidate the charge distributions in the clusters.

Keywords: Density functional investigation; Transitional metal–nitride clusters; Stabilities; Geometries; Photoelectron spectra

1. Introduction

Homonuclear metal clusters have been the focus of several theoretical and experimental studies during the last two decades [1–4]. Various molecular properties of those clusters as diverse as equilibrium geometries and total energies [1–5]; magnetic moments [6,7] and static polarizabilities [8] have been intensively investigated and calculated inter alia. Clusters under study have varied from small metallic dimers [8] to quite large systems having 30 transition metal atoms or over [7]. The theoretical methods employed in those studies have ranged from the relatively simple Jellium model, which has indeed provided a reasonable description for many metallic clusters [2,4], to ab initio density functional theory (DFT) and post-Hartree–Fock methods [6].

More recently [9], there has been a growing interest in synthesizing and studying relatively small metallic clusters containing a few non-metal atoms such as nitrogen and carbon. The relevance

* Corresponding author. Fax: +86-0551-5141078.
E-mail address: jghan@ustc.edu.cn (J.-G. Han).

0301-0104/$ - see front matter © 2003 Elsevier B.V. All rights reserved.
doi:10.1016/j.chemphys.2003.08.002

of those clusters lies in the prospect of developing new catalysts from cluster assembled materials involving nitrides, oxides and carbides of transition metals [10]. Those types of clusters can be also regarded as very small prototypes of a single molecule adsorbed on the metal surface of a heterogeneous catalyst. Therefore, theoretical studies of increasingly growing metallic clusters with a few adsorbed atoms or molecules can elucidate the variation of the adsorption and catalytic properties from the microscopic level to the bulk catalyst. Some interesting types of small metallic clusters bearing non-metal atoms are those containing transition metal and nitrogen atoms. One example of those systems is the series of adsorption complexes formed with the N_2 molecule and monomers and dimers of the transitions metals: Sc, Ti, V, Cr, Co and Ni [11]. Theoretical studies of those small systems are highly relevant for the catalytic processes involved in ammonia synthesis and nitrogen fixation [12]. A theoretical investigation on those clusters has been conducted at the level of the DFT [13] with the exchange and correlation potentials under both the local spin density approximation (LSDA) of Vosko–Wilk–Nussair (SVWN5) [14] and the generalized gradient approximation (GGA) of Becke–Perdew–Wang (BPW91) [13], and employing 6-311G* basis sets for all the atoms. It has been found in the course of that study that the adsorbed N_2 molecule was still characterized by a strong triple covalent bond that invariably remained unchanged after its adsorption on the metal clusters. On the other hand, the transition metal atoms had the d-orbitals partially unoccupied, with the energy cost to alter the atomic orbital populations being rather small. More importantly, the adsorption of the N_2 molecule on the transition metal clusters changed noticeably the magnetic character of the metal atoms, with transitions from anti-ferromagnetism to ferromagnetism in the case of the Cr clusters. The variation of the magnetic properties of metallic clusters upon N_2 adsorption has been observed in almost all the transition metal systems at varying degrees.

In other research areas, metallic clusters having a few nitrogen atoms in the nitride form are also relevant for catalytic purposes [10]. Several experimental studies on nitride metallic clusters have been conducted involving different transitions metals such as Ti, Zr and Nb [9]; Nb, Ta and Re, [15]; and Y and La [16]. Recently [17], a series of nitrogen-bearing copper clusters anions of the type Cu_nN^{-1} ($n = 2$–3), Cu_nNO^{-1} ($n = 1$–3) and $Cu_nNO_2^{-1}$ ($n = 1$–2) have been synthesized and characterized. All those clusters play important roles in the catalytic processes on Cu surfaces to transform NO_n species into non-pollutant products. To the best of our knowledge, no theoretical investigation on this series of interesting clusters has been conducted thus far. Therefore, the first systematic theoretical study on the $Cu_nN^{0,\pm1}$ ($n = 1$–4) clusters by DFT methods is reported herein as the first paper in a series of publications devoted to these types of compounds [18]. The present study includes the determination of the clusters equilibrium geometries and the calculation of their total energies, ionization potentials, electron affinities, fragmentation energies, natural orbital electron configurations, and Mulliken and natural orbital population analyses. Also, the photoelectron spectra of the Cu_nN^- ($n = 1$–4) anions have been calculated and the predicted results have shown a good agreement with the available experimental data [17]. The calculated properties have been employed in interpreting different chemical properties of the clusters such as their relative stability, the nature of their bonding, and their internal charge distributions inter alia.

2. Computational details

The explicit treatment of all the electrons in a cluster having a large number of atoms constitutes a demanding computational task. One of the best ways to surmount this difficulty is to make use of electron core potentials (ECP), also known as pseudo-potentials [19], by means of which only the valence electrons are explicitly treated. ECP calculations can actually provide accurate results for both homo- and heteronuclear clusters bearing transition metal, nitrogen, germanium or silicon atoms and their various combinations as firmly proven by previous investigations [20–22]. Therefore, the combination of DFT methods with ECPs

provides a feasible and accurate approach to the electronic structure study of the $Cu_nN^{0,\pm}$ ($n = 1$–4) clusters as shown below.

Present calculations were done at the level of the DFT theory with the hybrid Becke (B3) [23] exchange and the Lee, Yang and Parr (LYP) [24] correlation (B3LYP) functionals in combination with the Los Alamos ECP D95V [25] and double-zeta basis sets (LanL2DZ) [26] as implemented in the Gaussian 98 code [27]. Geometry optimizations of the $Cu_nN^{0,\pm1}$ ($n = 1$–4) clusters were systematically performed under the constraints of well-defined point-group symmetries and were followed by the evaluation of their harmonic vibrational frequencies in order to attest the clusters stability. Spin-polarized calculation for the Cu_nN ($n = 2$ and 4) and $Cu_nN^{\pm}$ ($n = 1$ and 3) clusters, and spin unpolarized calculation for the Cu_nN ($n = 1$ and 3) and $Cu_nN^{\pm}$ ($n = 2$ and 4) clusters were performed.

The combination of an ECP basis set with DFT exchange-correlation functionals might give rise to some reservations because those functionals were originally formulated for core and valence electron basis sets and not for ECP plus valence electron ones. However, the validity and accuracy of the present methodology have been established in the recent literature. For instance, Hagelberg et al. [28] compared DFT-B3LYP/LanL2DZ calculated geometries of several Si_n cages with well-established structures of those compounds and found a typical average deviation of 1–4% in bond lengths and angles. Furthermore, DFT-B3LYP/LanL2DZ ionization potentials of those Si_n cages agree satisfactorily with the DFT-B3LYP/6-311+G(d) results. In the same study, it was pointed out that the bond length of the Cu_2 molecule at the DFT-B3LYP/LanL2DZ level is of 2.26 Å, which deviates from the experimental result of 2.22 Å by less than 2% [28], and that the ionization potentials of Cu and Cu_2 at the DFT-B3LYP/LanL2DZ level are of 7.82 and 7.93 eV, which are in good agreement with the experimental values of 7.72 and 7.90 eV, respectively. In other series of studies [20], the calculated Cr–Cr bond length of Cr_2 at the DFT-B3LYP/LanL2DZ level turned out to be 1.61 Å, a value that compares well with the experimental one of 1.68 Å. The accuracy of this ECP approach in the case of the relevant N_2 molecule is discussed in the next section.

Given the somewhat preliminary nature of this investigation, the prediction of the clusters photoelectron spectra was performed by simply applying Koopmans theorem [13]: a satisfactory approach to treat the 3d electrons of the Cu atoms. Therefore, the use of the highly accurate outer valence Green function (propagator) (OVGF) methods [29,30] will not be used in this investigation but postponed to a future one [18]. Furthermore, a few comparisons between the Koopmans theorem and the OVGF spectra indicated that a relative error of about 9% in the spectra values can be expected when applying the Koopmans approach to these types of clusters. Comparisons of the calculated spectra with the experimental results give additional support to the use of the Koopmans theorem in the present context as shown below.

3. Results and discussion

The calculated properties for the $Cu_nN^{0,\pm1}$ ($n = 1$–4) clusters are presented in Tables 1–3. Equilibrium geometries and total energies are listed in Table 1; Mulliken population analysis charges, natural orbital population analysis charges and natural orbital electron configurations are listed in Table 2; ionization potentials (IP), electron affinities (EA) and fragmentation energies (FE) are listed in Table 3. Finally, the structures of the $Cu_nN^{0,\pm1}$ ($n = 1$–4) clusters are depicted in Fig. 1.

3.1. Equilibrium geometries, total energies, stability and photoelectron spectra

In order to assess the reliability and accuracy of the selected method and basis sets for the calculation of the $Cu_nN^{0,\pm1}$ ($n = 1$–4) clusters, the simpler N_2 molecule is first optimized at the DFT-B3LYP/LanL2DZ level; the obtained N–N bond length of 1.133 Å is in fair agreement with the reported computational and experimental results (1.107 and 1.098 Å, respectively) [8].

Table 1
Geometry and total energy of the $Cu_nN^{0,\pm1}$ ($n = 1$–4) clusters at the DFT-B3LYP/LanL2DZ level

Cluster	Symmetry	N–Cu(1)	N–Cu(4)	Cu(1)–Cu(2)	Cu(3)–Cu(4)	α	E_t
CuN	$C_{\infty v}$	1.800					−250.7044240
CuN^+	$C_{\infty v}$	1.878					−250.3925361
CuN^-	$C_{\infty v}$	1.816					−250.7948835
Cu_2N	C_s	1.867		2.343		60.0	−446.9204190
Cu_2N^+	C_s	1.800		2.594		161.5	−446.5352778
Cu_2N^-	C_s	1.827		2.361		4.4	−446.9508636
Cu_2N	$C_{\infty v}$	1.902		2.262		0.0	−446.8793980
Cu_2N^+	$C_{\infty v}$[a]	1.800		2.594		0.0	−446.5352778
Cu_2N^-	$C_{\infty v}$	1.833		2.362		0.0	−446.9508877
Cu_2N^+	$D_{\infty h}$[a]	1.813				180.0	−446.6626071
Cu_2N^-	$D_{\infty h}$	1.762				180.0	−446.9591470
Cu_2N	C_{2v}	1.861		2.750		95.3	−446.9669603
Cu_2N^+	C_{2v}	1.822		3.456		91.3	−446.6634761
Cu_2N^-	C_{2v}	1.833		2.621		143.0	−447.0040026
Cu_3N	C_{3v}	1.872		2.742			−643.1737007
Cu_3N^+	C_{3v}	1.855		3.213			−642.9398097
Cu_3N^-	C_{3v}	1.886		2.802			−643.2136482
Cu_3N	C_{2v}	1.815		2.430			−643.0636134
Cu_3N^+	C_{2v}	1.887		2.462			−642.8037220
Cu_3N^-	C_{2v}	1.837		2.406			−643.1502127
Cu_4N	C_{3v}	1.869	1.870	3.062	3.044		−839.3979666
Cu_4N^+	C_{3v}	1.864	1.860	3.046	3.041		−839.1582214
Cu_4N^-	C_{3v}	1.881	1.882	3.082	3.063		−839.4159645
Cu_4N	C_{2v}	1.878		2.440	2.394		−839.2922181
Cu_4N^+	C_{2v}	Second-order saddle point					
Cu_4N^-	C_{2v}	1.792		2.451	2.397		−839.3290114

Units: bond length, Å; Cu–N–Cu angle α, degree; total energy E_t, hartree.
[a] One imaginary frequency.

3.1.1. $CuN^{0,\pm1}$

$CuN^{0,\pm1}$ clusters of $C_{\infty v}$ symmetry are optimized at the DFT-B3LYP/LanL2DZ level; subsequent harmonic vibrational frequency analysis indicates that the three structures are stable. The Cu–N bond lengths for the CuN, CuN^- and CuN^+ clusters are: 1.800, 1.816 and 1.878 Å, respectively. The IP, EA and vertical ionization potential for the $^1\Sigma$ electronic-state CuN cluster are 8.487, 2.461 and 8.527 eV, respectively. Unlike the previously studied $CuSi_n$ clusters [31], the 3d atomic orbitals of the Cu atom in the $CuN^{0,\pm1}$ species do not behave as mere core orbitals but play an active role in bonding.

3.1.2. $Cu_2N^{0,\pm1}$

$Cu_2N^{0,\pm1}$ clusters under the constraints of the C_{2v}, $C_{\infty v}$, $D_{\infty h}$ and C_s, symmetries are optimized at the DFT-B3LYP/LanL2DZ level and are followed by harmonic vibrational frequency analyses. The converged $Cu_2N^{0,\pm1}$ structures of C_{2v} symmetry are found to be stable. Based upon the calculated results listed in Table 1, the Cu–N bond lengths of the ionic C_{2v} $Cu_2N^{\pm}$ clusters are shorter than those of the neutral C_{2v} Cu_2N cluster, a trend that is the opposite to that in the $CuN^{0,\pm1}$ series. Also, the Cu–Cu bond length (3.456 Å) of the C_{2v} Cu_2N^+ cation is longer than that of the neutral C_{2v} Cu_2N cluster (2.750 Å); but, conversely, the Cu–Cu bond length (2.621 Å) of the C_{2v} Cu_2N^- anion is shorter than that of the neutral C_{2v} Cu_2N cluster. Therefore, the Cu–Cu bond length in the C_{2v} $Cu_2N^{0,\pm1}$ series follows the relative order: $Cu_2N^+ > Cu_2N > Cu_2N^-$.

Geometry optimizations for the linear $C_{\infty v}$ $NCuCu^{0,\pm1}$ clusters series do converge although

Table 2
Mulliken and natural orbital population analysis charges, and natural orbital electronic configuration of the $Cu_nN^{0,\pm1}$ ($n = 1$–4) clusters at the B3LYP/LanL2DZ level

Cluster	Symmetry	Atom	Mulliken	Natural	Natural orbital electronic configuration
CuN	$C_{\infty v}$	Cu	0.333	0.525	[core] $4s^{0.69}3d^{9.73}4p^{0.05}$
		N	−0.333	−0.525	[core] $2s^{1.97}2p^{3.55}$
CuN^+	$C_{\infty v}$	Cu	0.903	1.003	[core] $4s^{0.31}3d^{9.68}4p^{0.01}$
		N	0.097	−0.003	[core] $2s^{1.98}2p^{3.01}$
CuN^-	$C_{\infty v}$	Cu	−0.470	−0.106	[core] $4s^{1.08}3d^{9.75}4p^{0.28}$
		N	−0.531	−0.891	[core] $2s^{1.96}2p^{3.93}$
Cu_2N	C_s	Cu(2)	0.091	0.042	[core] $4s^{0.97}3d^{9.96}4p^{0.02}$
		Cu(1)	0.190	0.410	[core] $4s^{0.78}3d^{9.75}4p^{0.05}$
		N	−0.281	−0.452	[core] $2s^{1.96}2p^{3.48}$
Cu_2N^+	C_s	Cu(2)	0.736	0.715	[core] $4s^{0.31}3d^{9.97}4p^{0.01}$
		Cu(1)	0.323	0.426	[core] $4s^{0.85}3d^{9.68}4p^{0.02}5p^{0.02}$
		N	−0.059	−0.141	[core] $2s^{1.97}2p^{3.17}$
Cu_2N^-	C_s	Cu(2)	−0.377	−0.585	[core] $4s^{1.63}3d^{9.93}4p^{0.01}5p^{0.01}$
		Cu(1)	−0.125	0.424	[core] $4s^{0.76}3d^{9.69}4p^{0.11}5p^{0.01}$
		N	−0.498	−0.839	[core] $2s^{1.95}2p^{3.89}$
Cu_2N	$C_{\infty v}$	Cu(2)	0.050	−0.121	[core] $4s^{1.44}3d^{9.66}4p^{0.02}$
		Cu(1)	0.210	0.570	[core] $4s^{0.82}3d^{9.55}4p^{0.05}$
		N	−0.261	−0.449	[core] $2s^{1.96}2p^{3.48}$
Cu_2N^+	$C_{\infty v}$	Cu(2)	0.736	0.715	[core] $4s^{0.31}3d^{9.97}4p^{0.01}$
		Cu(1)	0.323	0.426	[core] $4s^{0.85}3d^{9.68}4p^{0.02}5p^{0.02}$
		N	−0.059	−0.141	[core] $2s^{1.97}2p^{3.17}$
Cu_2N^-	$C_{\infty v}$	Cu(2)	−0.380	−0.586	[core] $4s^{1.63}3d^{9.93}4p^{0.01}5p^{0.01}$
		Cu(1)	−0.122	0.424	[core] $4s^{0.76}3d^{9.69}4p^{0.10}5p^{0.01}$
		N	−0.498	−0.838	[core] $2s^{1.95}2p^{3.89}$
Cu_2N^+	$D_{\infty h}$[a]	Cu	0.749	0.961	[core] $4s^{0.27}3d^{9.76}4p^{0.02}$
		N	−0.498	−0.922	[core] $2s^{1.92}2p^{3.99}3p^{0.01}$
Cu_2N^-	$D_{\infty h}$	Cu	−0.191	0.323	[core] $4s^{0.62}3d^{9.78}4p^{0.27}$
		N	−0.618	−1.645	[core] $2s^{1.83}2p^{4.81}3p^{0.01}$
Cu_2N	C_{2v}	Cu(1,2)	0.230	0.449	[core] $4s^{0.70}3d^{9.81}4p^{0.04}$
		N	−0.459	−0.898	[core] $2s^{1.94}2p^{3.95}3p^{0.01}$
Cu_2N^+	C_{2v}	Cu(1,2)	0.733	0.931	[core] $4s^{0.30}3d^{9.75}5p^{0.01}$
		N	−0.466	−0.862	[core] $2s^{1.93}2p^{3.93}3p^{0.01}$
Cu_2N^-	C_{2v}	Cu(1,2)	−0.224	0.118	[core] $4s^{0.96}3d^{9.76}4p^{0.16}$
		N	−0.551	−1.237	[core] $2s^{1.93}2p^{4.30}$
Cu_3N	C_{3v}	Cu(1–3)	0.202	0.462	[core] $4s^{0.66}3d^{9.82}4p^{0.03}5p^{0.03}$
		N	−0.606	−1.387	[core] $2s^{1.91}2p^{4.46}3p^{0.01}$
Cu_3N^+	C_{3v}	Cu(1–3)	0.588	0.795	[core] $4s^{0.35}3d^{9.84}4p^{0.02}$
		N	−0.765	−1.386	[core] $2s^{1.87}2p^{4.51}3p^{0.01}$
Cu_3N^-	C_{3v}	Cu(1–3)	−0.133	0.157	[core] $4s^{0.93}3d^{9.82}4p^{0.09}$
		N	−0.602	−1.470	[core] $2s^{1.94}2p^{4.50}\ 3s^{0.02}3p^{0.01}$
Cu_3N	C_{2v}	Cu(2,3)	0.158	0.079	[core] $4s^{0.92}3d^{9.95}4p^{0.02}5s^{0.01}5p^{0.02}$
		Cu(1)	0.024	0.461	[core] $4s^{0.74}3d^{9.72}4p^{0.02}5s^{0.01}5p^{0.06}$
		N	−0.340	−0.619	[core] $2s^{1.95}2p^{3.66}$
Cu_3N^+	C_{2v}	Cu(2,3)	0.362	0.303	[core] $4s^{0.73}3d^{9.93}4p^{0.04}$
		Cu(1)	0.313	0.556	[core] $4s^{0.77}3d^{9.61}4p^{0.05}$
		N	−0.036	−0.162	[core] $2s^{1.96}2p^{3.19}$
Cu_3N^-	C_{2v}	Cu(2,3)	−0.168	−0.298	[core] $4s^{1.28}3d^{9.94}4p^{0.05}5s^{0.02}5p^{0.01}$
		Cu(1)	−0.181	0.444	[core] $4s^{0.58}3d^{9.80}4p^{0.17}5s^{0.01}5p^{0.01}$
		N	−0.482	−0.847	[core] $2s^{1.92}2p^{3.92}$
Cu_4N	C_{3v}	Cu(1–3)	0.229	0.459	[core] $4s^{0.66}3d^{9.84}4p^{0.04}$
		Cu(4)	0.228	0.456	[core] $4s^{0.66}3d^{9.84}4p^{0.04}$
		N	−0.915	−1.834	[core] $2s^{1.87}2p^{4.93}3s^{0.02}3p^{0.02}$

Table 2 (*continued*)

Cluster	Symmetry	Atom	Mulliken	Natural	Natural orbital electronic configuration
Cu_4N^+	C_{3v}	Cu(1–3)	0.507	0.724	[core] $4s^{0.39}3d^{9.85}4p^{0.03}$
		Cu(4)	0.508	0.726	[core] $4s^{0.39}3d^{9.85}4p^{0.03}$
		N	−1.029	−1.799	[core] $2s^{1.80}2p^{5.07}3p^{0.02}$
Cu_4N^-	C_{3v}	Cu(1–3)	−0.043	0.211	[core] $4s^{0.88}3d^{9.84}4p^{0.07}$
		Cu(4)	−0.040	0.209	[core] $4s^{0.88}3d^{9.84}4p^{0.07}$
		N	−0.830	−1.842	[core] $2s^{1.97}2p^{4.83}3s^{0.02}3p^{0.02}$
Cu_4N	C_{2v}	Cu(1)	0.087	0.343	[core] $4s^{0.81}3d^{9.77}4p^{0.06}5s^{0.01}5p^{0.01}$
		Cu(2,3)	0.050	0.133	[core] $4s^{0.87}3d^{9.96}4p^{0.03}5s^{0.01}$
		Cu(4)	0.136	−0.052	[core] $4s^{1.05}3d^{9.93}4p^{0.06}$
		N	−0.320	−0.556	[core] $2s^{1.96}2p^{3.59}$
Cu_4N^-	C_{2v}	Cu(1)	−0.222	0.434	[core] $4s^{0.71}3d^{9.70}4p^{0.11}5s^{0.01}5p^{0.04}$
		Cu(2,3)	−0.154	−0.235	[core] $4s^{1.24}3d^{9.95}4p^{0.01}5s^{0.01}5p^{0.03}$
		Cu(4)	−0.096	−0.088	[core] $4s^{1.07}3d^{9.94}4p^{0.01}5s^{0.01}5p^{0.06}$
		N	−0.472	−0.882	[core] $2s^{1.94}2p^{3.93}$

[a] One imaginary frequency.

Table 3
Electron affinities (EA), ionization potential (IP) and fragmentation energy (FE) of the most stable $Cu_nN^{0,\pm1}$ ($n = 1$–4) clusters at the DFT-B3LYP/LanL2DZ level

Cluster	Symmetry	IP	EA	FE
CuN	$C_{\infty v}$	8.487	2.461	2.635
CuN^-	$C_{\infty v}$			–
CuN^+	$C_{\infty v}$			–
Cu_2N	C_{2v}	8.258	1.008	3.965
Cu_2N^+	C_{2v}			4.194
Cu_2N^-	C_{2v}			2.512
Cu_3N	C_{3v}	6.364	1.087	2.447
Cu_3N^+	C_{3v}			4.341
Cu_3N^-	C_{3v}			2.526
Cu_4N	C_{3v}	6.524	0.490	2.924
Cu_4N^+	C_{3v}			2.765
Cu_4N^-	C_{3v}			2.327

Units: eV for IP, EA and fragmentation energy FE.

frequency analysis on the Cu_2N^+ cation reveals one imaginary frequency: the converged structure corresponds to a transition state. The Cu–N bond length in the $C_{\infty v}$ Cu_2N^- anion is shorter than that of the neutral $C_{\infty v}$ Cu_2N cluster but the Cu–Cu bond length follows the reverse order. Furthermore, the Cu–N bond length (1.902 Å) in the linear $C_{\infty v}$ Cu_2N cluster is longer than that in the C_{2v} Cu_2N cluster (1.861 Å). Finally, the calculated HOMO–LUMO energy gaps (E_{gap}) in the Cu_2N clusters are 3.025 and 0.210 eV for the C_{2v} and $C_{\infty v}$ isomers.

Geometry optimization of the neutral $D_{\infty h}$ Cu_2N fails to converge. The converged $D_{\infty h}$ Cu_2N^+ structure exhibits one imaginary frequency but the converged $D_{\infty h}$ Cu_2N^- structure is found to be stable. Distortion of these more problematic geometries along the coordinate with imaginary frequency ultimately leads to the stable C_s $Cu_2N^{0,\pm1}$ structures listed in Table 1.

By comparing the calculated total energies of the neutral Cu_2N clusters of C_{2v}, $C_{\infty v}$ and C_s symmetries, the C_{2v} Cu_2N turns out to be the most stable structure. Moreover, the C_{2v} $Cu_2N^{\pm}$ clusters are lower in total energy than theirs $C_{\infty v}$, $D_{\infty h}$ and C_s counterparts. Finally, the IP and the EA of the most stable C_{2v} Cu_2N cluster are 8.258 and 1.008 eV, respectively, which are smaller than those of the CuN cluster.

Recently reported experimental photoelectron spectra of the Cu_2N^- clusters [17] have shown a peak at 1.0 eV and at the least four weak peaks in the range of 2.5–3.0 eV. These experimental results have also suggested that the experimentally observed Cu_2N^- consisted of at the least two different isomers. One of these isomers has three peaks at about 1.0, 2.7 and 3.0 eV. The present theoretical predictions for the photoelectron spectra of the Cu_2N^- anion show peaks at 2.542, 2.655 and 2.775 eV in the C_{2v} isomer; 2.601 and 2.614 eV in the $C_{\infty v}$ one; 0.872, 2.673, 2.682 and 3.014 eV in the $D_{\infty h}$ one; and finally, 1.609, 1.709, 1.710 and 1.961 eV in the C_s one. The calculated peaks of the different isomers of the Cu_2N^- anion in the range of 2.542–2.775 eV obviously correspond to the

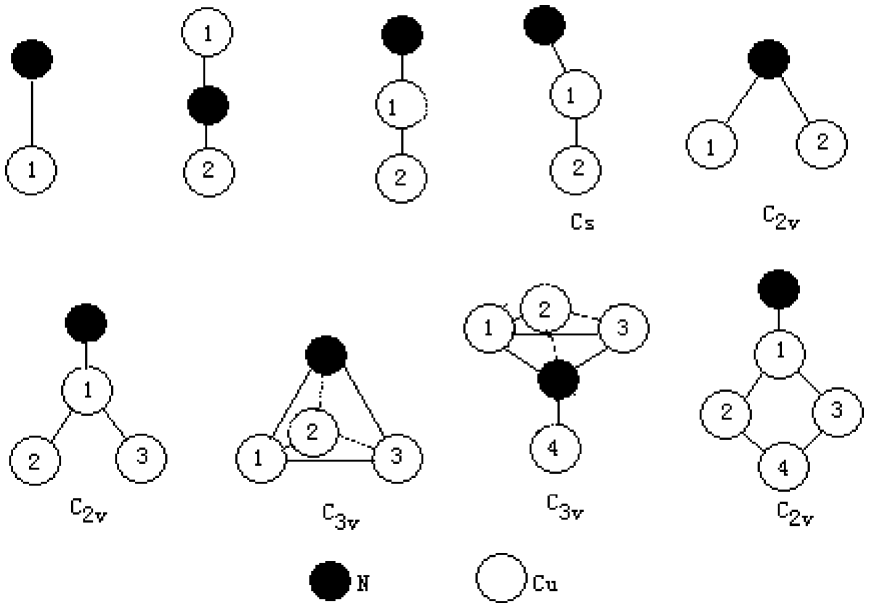

Fig. 1. The structures of $Cu_nN^{0,\pm1}$ ($n = 1$–4) clusters.

experimental data in the range of 2.5–3.0 eV [17]. The experimental peak at 1.0 eV can be assigned to the theoretical one at 0.872 eV of the $D_{\infty h}$ isomer, and the experimental peak at 3.0 eV to the theoretical one at 3.014 eV of the same isomer. On the whole, the ranges of values of the calculated photoelectron spectra are in good agreement with the available experimental results [17]: a fact that gives support to the use of the Koopmans theorem in the present context.

3.1.3. $Cu_3N^{0,\pm1}$

$Cu_3N^{0,\pm1}$ clusters under the constraints of the C_{3v} and C_{2v} symmetries are optimized at DFT-B3LYP/LanL2DZ level. Harmonic frequency analysis reveals that all the converged structures are stable. As in the case of the NH_3-like molecule, the N atom in the C_{3v} Cu_3N cluster is bonded to the three Cu atoms via sp^3 hybridization. In the case of the neutral C_{3v} Cu_3N, the Cu–N and the Cu–Cu bond lengths are of 1.872 and 2.742 Å, respectively, values that are comparable to those of the C_{2v} Cu_2N cluster. Comparison of the bond lengths in the C_{3v} $Cu_3N^{0,\pm1}$ series reveals that the Cu–Cu bond lengths in the ionic species are longer than that in the neutral one and that the Cu–N bond lengths follow the order: $Cu_3N^- > Cu_3N > Cu_3N^+$.

In the case of the C_{2v} $Cu_3N^{0,\pm1}$ clusters, the Cu(1)–N bond length follows the order: $Cu_3N^+ > Cu_3N^- > Cu_3N$, but the equivalent Cu(1)–Cu(2) and Cu(1)–Cu(3) bond lengths follows the order: $Cu_3N^+ > Cu_3N > Cu_3N^-$ instead. Also, in the Cu_3N and Cu_3N^- clusters, the Cu–N and the Cu–Cu bond lengths of the C_{3v} isomers are longer than those of the C_{2v} ones. However, in the cationic Cu_3N^+ cluster, the Cu–N bond length of the C_{3v} isomer is shorter than that of its C_{2v} counterpart.

The total energies (in hartrees) for the pairs of the C_{2v} and C_{3v} isomers are: −643.0636 and −643.1737 for the Cu_3N clusters; −642.8037 and −642.9398 for the Cu_3N^+ cations; and −643.1502, −643.2136 for the Cu_3N^- anions, respectively. In each pair, the C_{3v} $Cu_3N^{0,\pm1}$ isomer is lower in total energies than its C_{2v} counterpart. Therefore, the complete series of the $Cu_3N^{0,\pm1}$ clusters with C_{3v} symmetry is more stable. The IP and EA of the C_{3v} Cu_3N cluster are 6.364 and 1.087 eV, respectively, being its IP perceptibly smaller than those of the C_{2v} Cu_2N and CuN clusters.

Recent experimental results [17] have shown that the photoelectron spectra of the Cu_3N^- anion, which is presumably a mixture of C_{3v} and C_{2v} isomers, have a strong band at 2.9 eV with two weak shoulders at 1.7 and 2.1 eV, respectively [17]. There has not been any theoretical study to elucidate those photoelectron spectra thus far. Based upon the present theoretical investigation on the Cu_3N^- anions, two calculated peaks at 1.424 and 1.241 eV in the C_{3v} and C_{2v} isomers, respectively, should correspond to the experimental shoulder at 1.7 eV (with error deviations of 0.3 and 0.5 eV, respectively); meanwhile, two other calculated peaks at 1.923 and 1.954 eV in the C_{3v} and C_{2v} isomers, respectively, should correspond to the experimental shoulder at 2.1 eV (both with error deviations of 0.2 eV). The rest of the calculated spectra indicate that most of the peaks belonging to the 3d electrons of the Cu atoms in the C_{3v} and C_{2v} Cu_3N^- anions are in the range of 2.5–3.0 eV, with the most localized peaks at 2.7, 2.9 and 3.0 eV. These three last peaks obviously correspond to the strong band at 2.9 eV [17].

3.1.4. $Cu_4N^{0,\pm1}$

Geometry optimizations on the $Cu_4N^{0,\pm1}$ clusters with C_{3v} and C_{2v} symmetries are performed at the DFT-B3LYP/LanL2DZ level, followed by a vibrational frequency analysis. The three $Cu_4N^{0,\pm}$ converged structures with C_{3v} symmetry turn out to be stable. The Cu(1)–N and the Cu(4)–N bond lengths of the Cu_4N^+, Cu_4N^- and Cu_4N clusters with C_{3v} symmetry are 1.864 and 1.860 Å; 1.881 and 1.882 Å; and 1.869 and 1.870 Å, respectively. These values establish for both types of bonds the same relative order: $Cu_4N^- > Cu_4N > Cu_4N^+$. On the other hand, the Cu(1)–Cu(2) and Cu(3)–Cu(4) bond lengths for the Cu_4N^+, Cu_4N^- and Cu_4N clusters with C_{3v} symmetry are 3.046 and 3.041 Å; 3.082 and 3.063 Å; and 3.062 and 3.044 Å, respectively.

Vibrational frequency analysis revels that the converged C_{2v} Cu_4N^0 and Cu_4N^{-1} structures are stable but shows two imaginary frequencies in the case of the C_{2v} Cu_4N^+ cation. This last structure corresponds to a second-order saddle point. The Cu–N bond lengths in the stable Cu_4N and Cu_4N^- with C_{2v} symmetry are 1.878 and 1.792 Å, respectively. Also, the Cu(1)–Cu(2) and Cu(3)–Cu(4) bond lengths are 2.440 and 2.394 Å in the C_{2v} Cu_4N; and 2.451 and 2.397 Å in the C_{2v} Cu_4N^-, respectively.

Inspection of the calculated total energy indicates that all the $Cu_4N^{0,-1}$ species with C_{2v} symmetries are higher in energies than their C_{3v} counterparts. Therefore, the C_{3v} $Cu_4N^{0,\pm1}$ clusters are the most stable isomers. Also, the IP and EA of the C_{3v} Cu_4N cluster are 6.524 and 0.490 eV, respectively, which are smaller than those of the C_{2v} Cu_2N and $C_{\infty v}$ CuN clusters.

The calculated photoelectron spectra for the C_{2v} Cu_4N exhibit a peak at 1.10 eV belonging to the 2p atomic orbitals of the N atom, another peak at 1.227 eV belonging to the 4s atomic orbital of the Cu atom, and 11 peaks in the range of 2.7–3.0 eV corresponding to the 3d atomic orbitals of the Cu atom. On the other hand, the calculated photoelectron spectrum for the C_{3v} Cu_4N^- predicts three peaks at about 1.4 eV, four peaks at about 2.8 eV, five peaks at about 2.9 eV, and finally four peaks at about 3.0 eV. Unfortunately, no experimental photoelectron spectra for the Cu_4N^- clusters are available for comparison at present.

3.2. Fragmentation energies

For the Cu-atom abstraction reactions:

$$Cu_nN = Cu_{n-1}N + Cu$$
$$Cu_nN^+ = Cu_{n-1}N^+ + Cu$$
$$Cu_nN^- = Cu_{n-1}N^- + Cu$$

the successive fragmentation energies (FE): FE_N, FE_C and FE_A for the neutral Cu_nN, cationic Cu_nN^+ and anionic Cu_nN^- ($n = 1$–4) clusters can be defined as [32]:

$$FE_N = E_{Cu_{n-1}N} + E_{Cu} - E_{Cu_nN}$$
$$FE_C = E_{Cu_{n-1}N^+} + E_{Cu} - E_{Cu_nN^+}$$
$$FE_A = E_{Cu_{n-1}N^-} + E_{Cu} - E_{Cu_nN^-}$$

Calculated fragmentation energies for the most stable $Cu_nN^{0,\pm1}$ ($n = 1$–4) clusters at the DFT-B3LYP/LanL2DZ level are listed in Table 3. The FE_N values for the neutral species: CuN, C_{2v} Cu_2N, C_{3v} Cu_3N and C_{3v} Cu_4N are: 2.635, 3.965, 2.447 and 2.924 eV, respectively. These values

establish the following order for the relative stability of the neutral clusters with respect to Cu-atom abstraction: Cu_2N (C_{2v}) > Cu_4N (C_{3v}) > CuN > Cu_3N (C_{3v}). Also, the calculated FE_C values for the cations: C_{2v} Cu_2N^+, C_{3v} Cu_3N^+ and C_{3v} Cu_4N^+ are: 4.194, 4.341 and 2.765 eV, respectively; and the FE_A values for the anions: C_{2v} Cu_2N^-, C_{3v} Cu_3N^- and C_{3v} Cu_4N^- are: 2.512, 2.526 and 2.327 eV, respectively. The relative stabilities of the $Cu_nN^{\pm1}$ ($n = 2$–4) ions are therefore: $Cu_3N^{\pm1}$ (C_{3v}) > $Cu_2N^{\pm1}$ (C_{2v}) > $Cu_4N^{\pm1}$ (C_{3v}). In the $Cu_nN^{\pm1}$ ($n = 2$–4) ionic series, the C_{3v} $Cu_3N^{\pm1}$ ions are the most stable clusters with respect to Cu-atom abstraction, with the maximum stability belonging to the C_{3v} Cu_3N^{+1} cation.

3.3. Population analysis

Calculated Mulliken and natural orbital population analysis charges along with natural orbital electron configurations are listed in Table 2. Previous calculations on the MSi_n ($n = 1$–6; M = Cr, Mo, W) [20,33,34] clusters have proven that the natural orbital population analysis and the natural orbital electron configurations provide a more accurate description for the charge distributions in a cluster than the Mulliken population analysis. In the neutral CuN, the natural orbital charges of the Cu and the N atoms are 0.525 and −0.525, respectively. Removal of one electron from the CuN molecule to generate the CuN^+ cation makes the charges on the Cu and the N atoms become 1.003 and −0.003, respectively, with most of the total positive charge localized on the Cu atom as expected. Addition of one electron to the CuN molecule to generate the CuN^- anion makes the charges on the Cu and the N atoms become −0.106 and −0.8591, respectively, with now most of the charge excess localized on the N atom. Nonetheless, in the case of the CuN^- anion, neither the natural orbital charges nor the Mulliken ones agree fairly with the values predicted in [17].

In the case of the neutral C_{2v} Cu_2N, the natural orbital charges on the Cu and the N atoms are 0.449 and −0.898, respectively. In this molecule, the final charge distribution indicates that electrons originally localized on the 4s atomic orbitals of the Cu atom have been transferred to the 3d orbitals of the Cu and to the 2p orbitals of the N. In the cationic C_{2v} Cu_2N^+, the removed one-electron charge from the C_{2v} Cu_2N comes mainly from the 4s atomic orbitals of the Cu atoms because their electronegativity is lower that that of the N atom; this situation is similar to that in the CuN^+ cluster as discussed above. On the other hand, the negative charge excess in the C_{2v} Cu_2N^- anion localizes mainly on the 2p orbitals of the N atom. In the case of the $C_{\infty v}$ Cu_2N cluster, the charges on the N atom and on the more distant Cu atom [Cu(2)] are −0.449 and −0.121, respectively, with some negative charge transferred from the Cu(1) atom; In the case of the $C_{\infty v}$ Cu_2N^- anion, the extra one-electron charge mainly localizes on the N atom although some increase of negative charge on the Cu(2) atom is observed as well. Similar charge transfers are found in the other calculated clusters. The charge distributions in the present systems show a similar pattern to that in the Cu_2NO_2 clusters [18].

4. Conclusion and summary

Equilibrium geometries of the $Cu_nN^{0,\pm1}$ ($n = 1$–4) clusters under the constraint of well-defined point-group symmetries are optimized at the DFT-B3LYP level employing LanL2DZ basis sets. Total energies, ionization potentials and electron affinities are presented and discussed. The photoelectron spectra of the anionic Cu_nN^- ($n = 2$–4) clusters are calculated via Koopmans theorem, with the predicted values exhibiting a good agreement with the available experimental data [17]. A more detailed analysis of those calculated photoelectron spectra for the Cu_nN^- ($n = 2$–4) clusters reveals that the predicted energy differences of more than 1 eV between the 3d and 4s atomic orbitals of the Cu atom and between the 3d atomic orbitals of the Cu atom and the 2p of the N atom are also in good agreement with the experimental results [17]. In addition, the relative stabilities of the $Cu_nN^{0,\pm1}$ ($n = 1$–4) clusters with respect to Cu-atom abstraction are determined from their fragmentation energies. Those theoretical results indicate that the cationic Cu_nN^+ ($n = 1$–4) clusters are more stable than

their anionic Cu_nN^- counterparts, with the C_{3v} Cu_3N^+ cluster being the most stable cluster in the present series. Mulliken and natural orbital population analysis charges, and natural orbital electron configurations are also calculated. The theoretical results reveal that the negative charge excess in the Cu_nN^- clusters is mainly localized on the 2p atomic orbitals of the N atom, and that the removed charge in the Cu_nN^+ clusters comes mainly from the 4s atomic orbital of the Cu atoms. Also, charge transfers from the 4s orbitals of the Cu atoms to the 2p orbitals of the N atom are observed in all the investigated clusters.

Acknowledgements

This work is supported by a research fund from the Structural Research Laboratory of the University of Science and Technology of China at Hefei (2001B10), the National Foundation from the Department of Science and Technology of China (970211006), the National Natural Science Foundation of China (20173055), the Robert A. Welch Foundation (USA) and the Research Corporation (USA). One of the authors (H.J.G.) is indebted to Dr. D.J. Fox (Gaussian, Inc. USA) and Dr. F. Misaizu (Department of Chemistry, Tohoku University, Japan) for their useful discussions.

References

[1] M.D. Morse, Chem. Rev. 86 (1986) 1049.
[2] M.L. Cohen, M.Y. Chou, W.D. Knight, W.A. de Heer, J. Phys. Chem. 91 (1987) 3141.
[3] M.M. Kappes, Chem. Rev. 88 (1988) 369.
[4] W.A. de Heer, Rev. Mod. Phys. 65 (1993) 611.
[5] A. Daoudi, A.T. Benjelloun, J.P. Flament, G. Berthier, J. Mol. Spectrosc. 194 (1999) 8.
[6] B.V. Reddy, S.N. Khanna, B.I. Dunlap, Phys. Rev. Lett. 70 (1993) 3323.
[7] A.J. Cox, J.G. Louderback, L.A. Bloomfield, Phys. Rev. Lett. 71 (1993) 923.
[8] E.J. Moler, S.A. Kellar, W. Huff, Z. Hussain, Y.E. Zheng, et al., Chem. Phys. Lett. 264 (1997) 502.
[9] S.E. Kooi, A.W. Castleman, Chem. Phys. Lett. 315 (1999) 49.
[10] S.T. Oyama, The Chemistry of Transition Metals Carbides and Nitrides, Blackie, London, 1996.
[11] S.W. Weber, B.V. Reddy, B.K. Rao, P. Jena, Chem. Phys. Lett. 295 (1998) 175.
[12] G.L. Miessler, D.A. Tarr, Inorganic Chemistry, Prentice Hall, Englewood Cliffs, 1991.
[13] R.G. Parr, W.T. Yang, Density Functional Theory of Atoms and Molecules, Oxford University Press, New York, 1989.
[14] S.H. Vosko, L. Wilk, M. Nusair, Can. J. Phys. 58 (1980) 1200.
[15] M.F. Zhou, L. Andrews, J. Phys. Chem. A 102 (1998) 9061.
[16] G.V. Chertihin, W.D. Bare, L. Andrews, J. Phys. Chem. A 102 (1998) 3697.
[17] F. Misaizu, M. Furuhashi, A. Takada, Y. Yamakita, K. Ohno, Eur. J. Phys. D 9 (1999) 297.
[18] J.G. Han, J.A. Morales, in preparation.
[19] M. Krauss, W.J. Stevens, Ann. Rev. Phys. Chem. 35 (1984) 357.
[20] J.G. Han, F. Hagelberg, Chem. Phys. 263 (2001) 255.
[21] J.G. Han, Y. Shi, Chem. Phys. 266 (2001) 33.
[22] J.G. Han, Chem. Phys. 286 (2003) 181.
[23] A.D. Becke, J. Chem. Phys. 98 (1993) 1372.
[24] C. Lee, W. Yang, R.G. Parr, Phys. Rev. B 27 (1988) 785.
[25] H. Dunning Jr., P.J. Hay, in: H.F. Schaefer III (Ed.), Modern Theoretical Chemistry, vol. 3, Plenum Press, New York, 1976, p. 1.
[26] P.J. Hay, W.R. Wadt, J. Chem. Phys. 82 (1985) 270; W.R. Wadt, P.J. Hay, J. Chem. Phys. 82 (1985) 284; P.J. Hay, W.R. Wadt, J. Chem. Phys. 82 (1985) 299.
[27] M.J. Frisch, G.W. Trucks, H.B. Schlegel, G.E. Scuseria, M.A. Robb, J.R. Cheeseman, V.G. Zakrzewski, J.A. Montgomery Jr., R.E. Stratmann, J.C. Burant, S. Dapprich, J.M. Millam, A.D. Daniels, K.N. Kudin, M.C. Strain, O. Farkas, J. Tomasi, V. Barone, M. Cossi, R. Cammi, B. Mennucci, C. Pomelli, C. Adamo, S. Clifford, J. Ochterski, G.A. Petersson, P.Y. Ayala, Q. Cui, K. Morokuma, D.K. Malick, A.D. Rabuck, K. Raghavachari, J.B. Foresman, J. Cioslowski, J.V. Ortiz, B.B. Stefanov, G. Liu, A. Liashenko, P. Piskorz, I. Komaromi, R. Gomperts, R.L. Martin, D.J. Fox, T. Keith, M.A. Al-Laham, C.Y. Peng, A. Nanayakkara, C. Gonzalez, M. Challacombe, P.M.W. Gill, B. Johnson, W. Chen, M.W. Wong, J.L. Andres, C. Gonzalez, M. Head-Gordon, E.S. Replogle, J.A. Pople, Gaussian 98, Pittsburgh, PA, 1998.
[28] F. Hagelberg, C. Xiao, W.A. Lester Jr., Phys. Rev. B 67 (2003) 35426.
[29] J.V. Ortiz, J. Chem. Phys. 89 (1988) 6348.
[30] L.S. Cederbaum, J. Phys. B 8 (1975) 290.
[31] F. Hagelberg, I. Yanov, J. Leszczynski, J. Mol. Struct. (THEOCHEM.) 487 (1999) 183.
[32] J.G. Han, Chem. Phys. Lett. 324 (2000) 143.
[33] J.G. Han, F. Hagelberg, J. Mol. Struct. (THEOCHEM.) 549 (2001) 165.
[34] J.G. Han, F. Hagelberg, Struct. Chem. 13 (2002) 173.